Mechanical Systems and Signal Processing (2003) **17**(5), 1033–1047
doi:10.1006/mssp.2002.1530

FAULT DETECTION IN GEAR DRIVES WITH NON-STATIONARY ROTATIONAL SPEED—PART I: THE TIME–FREQUENCY APPROACH

G. Meltzer

Dresden University of Technology, Faculty of Mechanical Engineering, Department of Energy Machines and Machine Laboratory, Technical Diagnostics, D-01062 Dresden, Germany. E-mail: meltzer@mal.mw.tu-dresden.de

AND

Yu Ye Ivanov

ZF Friedrichshafen, Germany

(Received 1 February 1999 September 2002, accepted after revisions 23 September 2002)

This paper deals with the recognition of faults in toothing during non-stationary start-up and run-down of gear drives. In the first part, this task will be solved by means of the time–frequency analysis. As a practical case study, we investigated a planetary gear for passenger cars. New exponental smoothing kernels which respect to the known-in-advance angular acceleration of gear drive were created. These kernels must be adapted in the case of an in-advance-unknown course of rotational speed.

1. INTRODUCTION

This paper is a result of our investigation in connection with the quality management of passenger car gearing drives. For saving time and costs, these gears are subjected to quick tests with automatically changed load and speed on test rigs at the producers shop. It means, that no time interval, in which the rotational speed is steady exists. Because of this an ordinary Fourier transformation cannot be applied. But—as it will be shown later—by means of an incremental sensor the time-equidistant sampling can be replaced by a sampling with constant intervals along the rotational angle axis. When the gear drives will be checked in repair shops after a certain time of exploitation, no incremental sensors will be available. Therefore, a new approach for analysing measured vibration signals under non-stationary condition must be found.

The traditional approach for checking of gears is an acceleration measurement with Fourier transformation, sideband analysis, envelope analysis or cepstral transformation on the basis of time-equidistant sampling. But these procedures are not appropriate in our case because of the unsteady rotational speed [1–3]. Their application can lead to false diagnostic results as shown in Section 5.1 of our paper. Considering this, we distinguish between sampling with equidistant rotational angle intervals (see Section 4) and with time-equidistant sampling (see Section 5).

One of the data processing methods, which allows a precise analysis of unsteady time series $x(t)$, is the method of time–frequency analysis (TFA) [1–3]. The result of this analysis is a set of temporary spectra along the time axis, the so-called time–frequency distribution

0888–3270/03/ + $30.00/0

$TFD_X(t;\omega)$. Quadratic forms of TFD lead to the joint temporary distribution of signal energy along the time-axis and the frequency-axis. On the field of gear diagnostics mostly the TFA of Cohen class [4–6] as well as wavelets [7, 8] are applied. We confine ourself in this paper to the application of Cohen class.

Already there exist many reports about the diagnosis of faults or damages in gear drives [4–6, 9, 10]. The investigated damages were pittings at the tooth flank as well as partially cracked teeth. The TFD plot of measured structure-borne noise shows in these cases free vibrations, which are generated by meshing of damaged teeth as well as modulations of forced vibration with the meshing frequency. For identification of different damages here, we used methods of automatic image recognition [5].

All papers, which we have found until now, described the detection of faults via the analysis of short transient vibration midst of a stationary acceleration signal, which was generated by the tooth meshing with steady rotational speed [4–6, 9]. In contrast to this approach, we tried to solve the task of fault diagnosis of gears at strong unsteady rotational speed, which was caused by the special unsteady controlled test runs in the factory.

Our paper is divided in two parts. Part I is focused on the fault detection by means of TFA. It consists of six sections. The first section is an introduction. The second section is a short survey of TFA on the basis of Cohen-class distributions. Section 3 describes the practical aspects of the treated case study (the passenger—car planetary gearing drive) and the measuring technique. Sections 4 and 5 are the central parts: they describe the processing of angle- and time-equidistant sampled time functions and its results. Section 6 is a summary.

Part II appears in a later issue of MSSP. It deals with the quefrency–time approach to the same problem.

2. TFA ON THE BASIS OF DISTRIBUTIONS OF COHEN CLASS

The Cohen class involves quadratic TFA, which are invariant with regard to time and frequency shifts. They are for the first time published by Cohen [1, 3]. Each member $TFD_X(t;\omega)$ of this class can be described by a general formula

$$TFD_x(t;\omega) = (1/2\pi)\int_{-\infty}^{+\infty}\int_{-\infty}^{+\infty} A_x(\nu;\tau)H(\nu;\tau)\exp(-j\nu t)\exp(-j\omega\tau)\,\mathrm{d}\nu\,\mathrm{d}\tau \tag{1}$$

with $Ax(\nu;\tau)$ as the ambiguity function (AF) of the time function $x(t)$:

$$A_x(\nu;\tau) = \int_{-\infty}^{+\infty} x^*(t-\tau/2)x(t+\tau/2)\exp(j\nu t)\,\mathrm{d}t. \tag{2}$$

We can see from equation (1), that each type of TFD of Cohen class is determined by its specific integral kernel $H(\nu;\tau)$. The kernel $H_{WVV}(\nu;\tau) = 1$ belongs to the Wigner–Ville distribution (WVD), the kernel $H_{\mathrm{CWV}}(\nu;\tau) = exp[-\nu^2\tau^2/(4\pi^2\sigma)]$ to the Choi–Williams distribution (CWD) and

$$H_{SP}(\nu;\tau) = \int_{-\infty}^{+\infty} w^*(t-\tau/2)w(t+\tau/2)\exp(j\nu t)\,\mathrm{d}t$$

belongs to the spectrogram. $w(t)$ is the specific time window, which is used for calculation of the spectrogram [2, 11, 12].

The selection of the TFD is influenced by the aim to find an optimum between the resolution in time and frequency on one side and the suppression of interference terms, which are generated by every kind of Cohen-class distributions, on the other side. This aim shall be explained in more detail for spectrograms, WVD and CWD now.

The so-called spectrogram shows the lowest resolution, but a nearly perfect smoothing of interference terms* [1, 12]. Figure 1(a) shows the contour plot of the kernel $H_{SP}(\nu;\tau)$ of a spectrogram. It embraces a small region around the origin of the $\{\nu;\tau\}$ plane only. By weighting of the AF $A_x(\nu;\tau)$ of the measured signal, $x(t)$, with this kernel, only those terms of product $A_x(\nu;\tau)H_{SP}(\nu;\tau)$ will exist furthermore, which are situated in this region. All interference terms lie out of the $\{\nu;\tau\}$ origin [1–3]. They will be totally suppressed and will no longer appear in the spectrogram. This is the reason for the absence of nearly all kinds of interferences in spectrograms. As a consequence, all components of signal that are situated far from the central region will be 'killed' by this kernel. The result is a limited resolution of spectrograms in time and frequency.

The WVD is characterised by the best resolution of all Cohen-class members. But it does not suppress any interference term in any way. With the kernel $H_{\mathrm{WVV}}(\nu;\tau) = 1$, the WVD is the only un-weighted TFD of the Cohen class. All other kinds of Cohen class distributions stand between both these and have a medium position with regard to the ratio 'resolution in time and frequency/damping of interference terms'.

It must be remarked that the efficiency of interference term suppression depends also on the special kind of measured signal. This is caused by the signal independence of kernels. CWD allows a good smoothing for stationary signals as well as for such transients that have changing magnitudes in course of time (but not for real chirps) [3]. The contour plot of CWD ($\sigma = 0.05$) is shown in Fig. 1(b). It embraces both axes in the ambiguity plane $\{\nu;\tau\}$. As is well known, all stationary components of the measured signal are situated along the τ-axis [3, 12], it means, in the central region. Amplitude-modulated transients are situated along the ν-axis, it means, also midst the central region of the CWD kernel $H_{\mathrm{CWV}}(\nu;\tau)$. By executing the mathematical operation $A_x(\nu;\tau)H_{\mathrm{CWV}}(\nu;\tau)$ in equation (1), both these kinds of signal components are preferred. All other components, which are situated far from the central region in the ambiguity plane, are relatively strongly suppressed. They will not make their appearance in CWD. On these considerations, we chose the application of CWD for the processing of digitalised measuring values, which were sampled in equidistant intervals of rotational angles. They appear as steady in the course of the rotational angle axis. For such kind of signals, whose terms are partially situated out of the τ- or ν-axis (here are the time-equidistant sampled signal of gear start-up or run-down as a kind of 'chirps' included), the CWD seems to be not so efficient [12]. Furthermore, we expect also some problems.

3. EXPERIMENTAL INVESTIGATIONS OF A GEAR DRIVE

Figure 2 shows the kinematic scheme of the investigated passenger-car gear drive. It has three planet sets (1), (2) and (3) with the transmission ratios $i_1 = 1.6329$, $i_2 = 0.6207$ and $i_3 = 3.0588$ resp. in a housing (4). Each of the planet set consists of one central gear wheel, one annulus wheel (ring wheel) and three planet wheels with a common planet carrier.

The experimental investigation was executed at an automatically controlled test rig in the producer's factory. The driving shaft (5) came from a fluid coupling. The structure-borne noise was picked up by an ordinary piezoelectric accelerometer (6). The measured signal was digitalised subsequently. This was tuned alternatively by an incremental sender (8) at the output shaft (7), which gave 2048 impulses per revolution in constant angular intervals, or by an ordinary impulse generator with constant time intervals. The investigated copy of gears did not pass the quality test because of a severe concentrated

*There exist interference terms in a spectrogram according to [13] only in such cases, if two different signal components are crossing each other in the time–frequency plane.

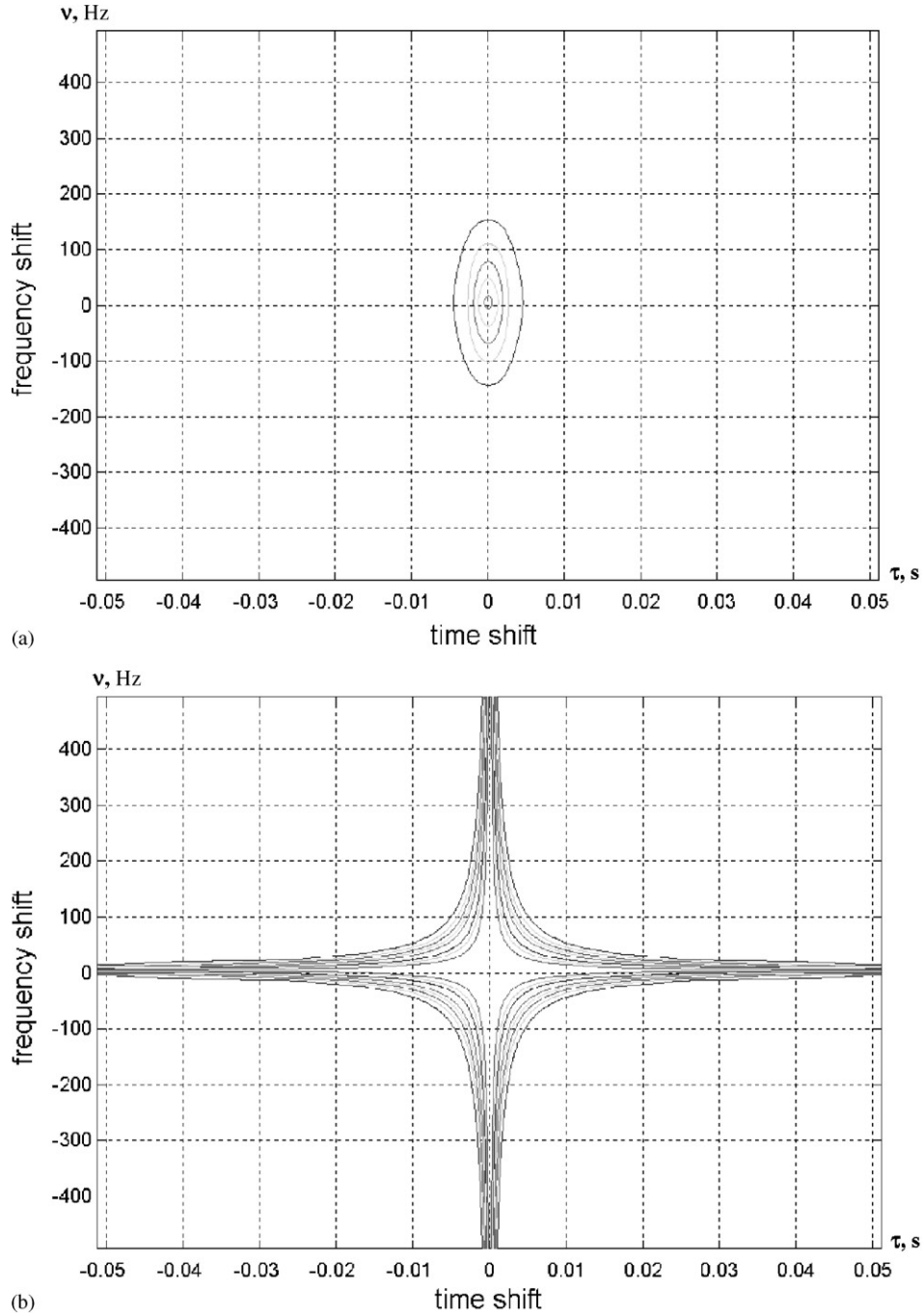

Figure 1. Kernels $H(v;\tau)$ of spectrogram (a) and CWD (b) in the ambiguity plane.

fault at the flank of one tooth of the central gear of the second planet set. The number of teeth were given by $z_{S2} = 54$, $z_{H2} = 87$, $z_{P2} = 16$. The wheels of the second set had the following rotational speeds ratios related to the output shaft: $i_{S2} = 3.058824$, $i_{H2} = 1.89858$, $i_{P2} = 10.323529$.

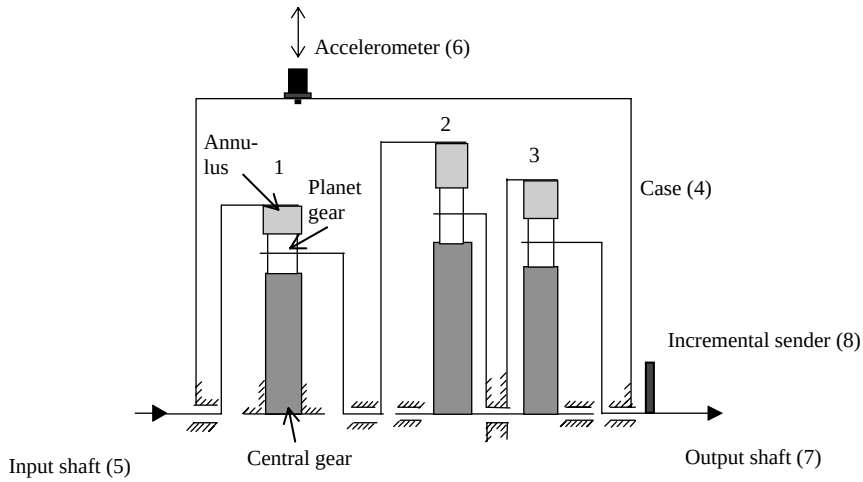

Figure 2. Kinematic schema of the investigated passenger car gear with three sets of planet gear (1, 2, 3).

The measuring was done during 16 revolutions of the output shaft with a measuring time interval of about $t_A = 1.13\,s$. In this interval, the rotational speed increased from ca.720 μm/min ($f_{AB} = 12.0$ Hz) to ca. 980 μm/min ($f_{AE} = 16.3$ Hz). The constant time interval for sampling was $\Delta t = 34.5$ μs. 32 768 digitalised measuring values at discrete time points were stored. The result is an unsteady time series. Besides this, 32 768 values in constant angular steps, $\Delta\varphi = 0.176^\circ$, were also additionally stored. This series of values is also unsteady relative to time axis, but nevertheless it is stationary relative to the rotational angle axis (not taking into consideration the changing of magnitudes during start-up).

4. PROCESSING OF THE ANGLE-EQUIDISTANT SAMPLED SIGNALS

Because of the stationarity relative to rotational angle values, the angle-equidistant sampled signals can be processed with the conventional methods of frequency analysis. But the result of the ordinary discrete Fourier-analysis is the ordering spectrum now, not the frequency spectrum of time series [14]. The TFA consequently leads to the time-ordering distribution (TOD) and not the TFD.

4.1. SPECTRAL AND CEPSTRAL ANALYSES

Figure 3(a) shows the measured signal consisting of 32 768 values in constant angle distances of $\Delta\varphi = 0.176^\circ$ of the output shaft. Figure 3(b) shows the corresponding ordering spectrum. The first order corresponds to the rotational frequency of the output shaft. The dominating peak is situated near the 165.2th order. This is the order of teeth meshing at the second planet set with the sun wheel as well as with the ring gear, because the planet carrier of the second planet set is clamped ($i_{S2}z_{S2} = i_{H2}z_{H2} = i_{P2}z_{P2} = 165.2$). There are no peaks recognisable near the meshing order of first and third planet sets (94.9th and 70th order). The reason is a resonance of the second set meshing frequency with one of the housing eigenfrequencies, presumably.

There are also some sidebands around the second set meshing order recognisable. But it is impossible to find any relation to the rotational orders of the wheels in the second set. In order to identify these sideband distances, the power cepstrum of the ordering spectrum was calculated [see Fig. 3(c)]. Two dominating quefrencies belong to the central wheel (0.327th ordering quefrency, denoted by 'C') and annulus (0.527th ordering quefrency,

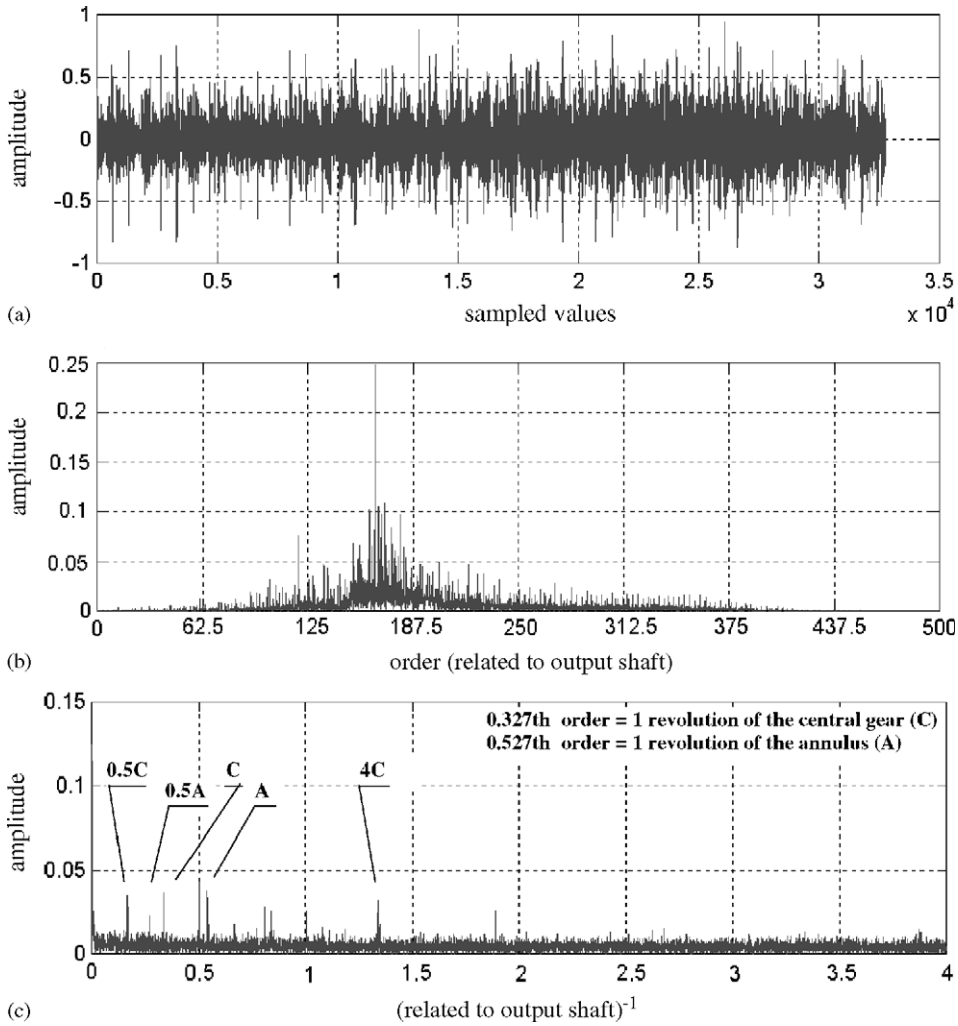

Figure 3. Angle-equidistant sampled signal of accelerometer at the gearbox (a), ordering spectrum (b) and cepstrum (c).

denoted by 'A'). The half-orders in cepstrum correspond to higher harmonics in ordering spectrum. These are also well-known symptoms for damaged tooth flanks. The higher rahmonics are generated by numerical calculation of logarithms.

There occur also two rahmonics, which correspond to the first and second harmonics of the output shaft. Perhaps they mark sidebands, which are generated by a non-uniform torque or rotational speed of the output shaft. The source of this can be a misaligment or something else. Whatever this may be, the diagnostics of gear drive with all symptoms is not the main topic of our paper. Let this appearance be furthermore out of consideration.

Summing up the results of ordering spectral analysis and ordering cepstral analysis, we confirmed the already identified fault at the sun wheel. But we detected additionally a fault also at the tooth flanks of annulus. This fault could not be confirmed unfortunately because of the dismantling of the concerned gear box meanwhile carried through.

This statement can also be confirmed by the analysis of the sharp peak near the 120th order [see Figure 3(b)]. This can now be identified as sideband of the meshing frequency

with distance correlating with the fifth harmonics of the repetition frequency of sun-wheel faults or with the eighth harmonics of the repetition frequency of annulus faults. When both of these damages exist, by their superposition, the recognised peak can be generated.

4.2. TIME-ORDERING ANALYSIS

Because of the stationarity of the measured signal according to the angle intervals, the CWD is suitable for calculating time-ordering distribution. It was numerically calculated according to formulas (1) and (2). The result of CWD calculation with a smoothing factor $\sigma = 0.05$ for 3 revolutions of output shaft (between the 26 624th and 32 768th sample—this corresponds to a time interval of ca. 0.212 s) is shown in Fig. 4 (as result of changing the display timescale only one revolution is shown here). During this time interval, the rotational speed increased from ca. 936 rpm ($f_{AM} = 15.6$ Hz) to ca. 980 rpm ($f_{AE} = 16.3$ Hz). Some marked perpendicular straight lines, which exist over the full measuring time can be recognised. These are the meshing frequency of the second planet set found already by means of ordering spectra and the sidebands of central gear and annulus. The dominating 165.2nd and 155.6th orders are the meshing frequency and the fifth sideband of annulus. The existing sidebands are very densily concentrated, interference terms are not recognisable. This is the result of appropriate choice of integral kernel $H_{\mathrm{CWV}}(v;\tau)$ in equation (1): the CWD provides a high level of resolution in time and frequency as well as of interference term suppression.

The additional horizontal lines in Fig. 4 seem to appear non-periodically or have a complicated structure of periodicity. These are perhaps generated by impacts between tooth flanks because of damages (such kind of impacts can be generated in the case of severe flank faults by the mutual influence of clearance and small load as well as of reduced

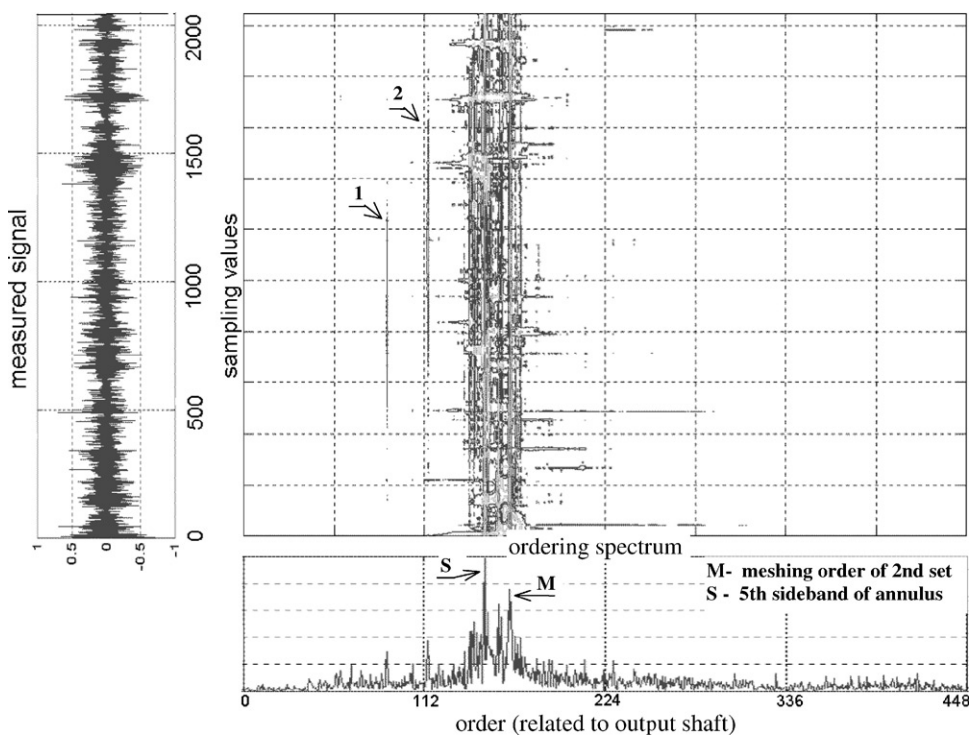

Figure 4. CWD with $\sigma = 0.05$ for three revolutions of the angle-equidistant sampled measuring signal at the gearbox ('1' and '2' mark individual sidebands).

contact stiffness and high load). Their significance for fault diagnosis was until now not investigated, but a research in this field could be very interesting and promising. The authors intend to publish new results in this field later.

5. PROCESSING OF TIME-EQUIDISTANT SAMPLED SIGNALS

The strong non-stationarity of the measured signals, caused by a fast start-up (or run-down) during gear drive testing, is their characteristic property. It creats the difference in data processing of time-equidistant sampled signals in comparision with angle-equidistant sampled ones.

5.1. SPECTRAL ANALYSIS AND CEPSTRAL ANALYSIS

The time-equidistant (with $\Delta t = 34.5\,\mu s$) sampled signal in Fig. 5(a) differs from the angle-equidistant sampled one in Fig. 3(a) only is the manner of sampling.

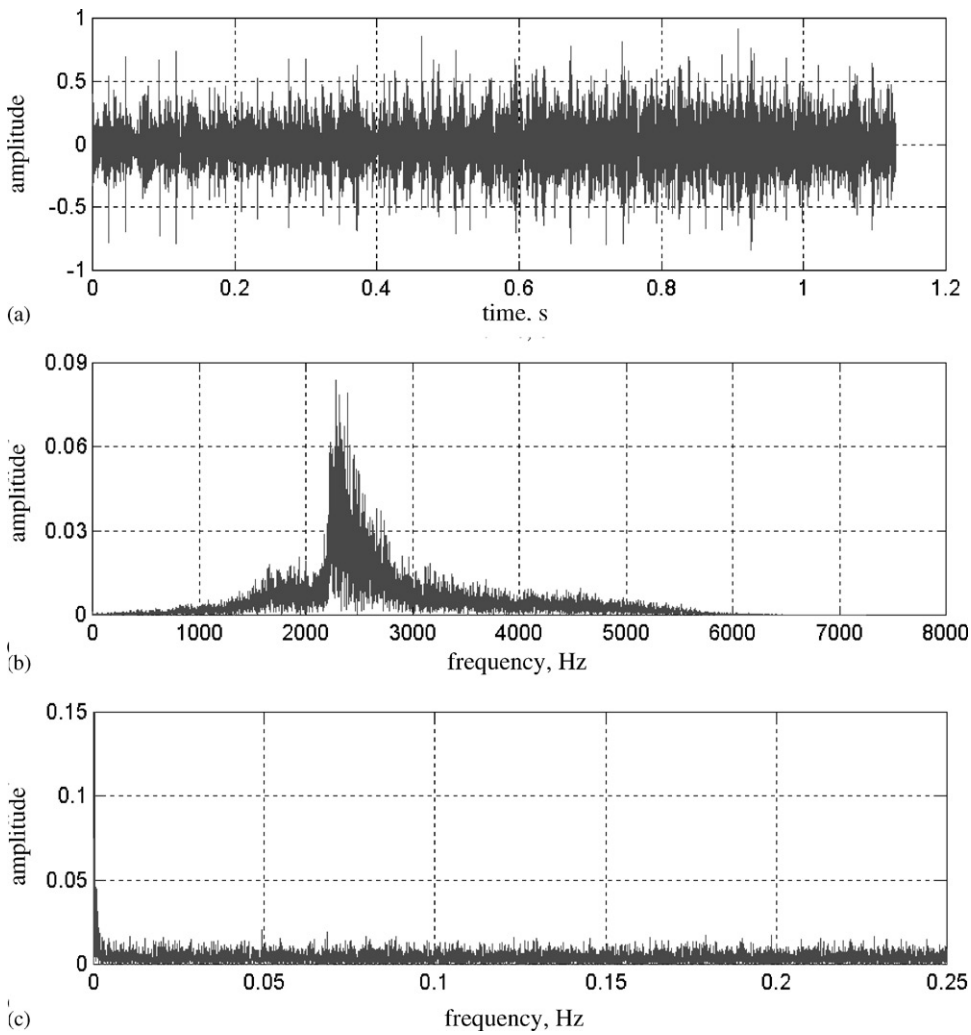

Figure 5. Time-equidistant sampled signal of accelerometer at the gearbox (a), frequency spectrum (b) and cepstrum (c).

The frequency spectrum of this signal in Fig. 5(b) looks very different in comparison with the ordering spectrum Fig. 3(b). All the peaks are smeared over, they cannot be distinguished.

The reason of this is the time dependence of meshing frequency and sideband distances [14, 15]. The conventional frequency analysis is not suitable for processing of such nonstationary signals. No peak can be identified in Fig. 5(b).

Also the power cepstrum does not improve this situation. As a consequence of the growth of rotational speed from 720 to 980 rpm during the measuring time interval, the quefrencies of sideband distances must decrease by ca. 26% (for the central gear from 0.027 to 0.020 s; for the annulus from 0.044 to 0.032 s). But Fig. 5(c) does not show any peak in these intervals. The conclusion of this cepstral analysis is that this gear is not of best quality: we know already that this copy has faults at the annulus flanks as well as at the sun wheel. Now it is evident that the Fourier-transformation as well as the cepstral analysis are not applicable for diagnosis of unsteady running machines.

5.2. THE TFA WITH ROTATIONAL SPEED-ADAPTED INTEGRAL KERNELS

In the case of numerically controlled test rigs with linearly changing rotational speed, the angular acceleration can be determined in advance. For our case- study subject, the meshing frequency of second planet set increases during the observed three revolutions with a measuring time interval $T = 0.212$ s from ca. $f_{Z1} = f_{AM} i_{S2} z_{S2} = 2564$ Hz to ca. $f_{Z2} = f_{AE} i_{S2} z_{S2} = 2698$ Hz (with $f_{AM} = 15.6$ Hz and $f_{AE} = 16.3$ Hz, see Section 4.2). The corresponding constant angular acceleration is ca. $\varepsilon_Z = 2\pi(f_{Z2} - f_{Z1})/T = 3983\,\mathrm{s}^{-2}$. All observable sidebands near the meshing frequency have nearly the same angular acceleration.

In our case of a gear with linearly increasing rotational speed, we expect a multi-component chirp also having linearly increasing meshing frequency and accompanying sidebands. The components of this chirps have to be characterised by parallel straight lines, which have to be inclined against the time axis according to the angular acceleration.

Figure 6 shows the CWD of the time-equidistant sampled signal, which was calculated with the ordinary integral kernel (see Section 2). While the straight lines in Fig. 4 are exactly perpendicular and go from the beginning to the end of measuring time-interval, the straight lines in Fig. 6 have a small inclination (but not so much as expected). Further they are interrupted along the time axis and also a little bit smeared over (see especially these regions in Figs 4 and 6, which are marked '1' and '2'). This is the result of divergence between the ambiguity function of the chirp and the situation of the ordinary Choi–Williams kernel in the time–frequency plane. Therefore, we will make evident in Part II of our paper that the CWD does not enable the detection of faults in gears with changing rotational speed.

As a conclusion of this result, we created an integral kernel $H(\nu;\tau)$, which has a similar geometry as the ambiguity function of the measured signal. For an efficient time–frequency analysis of chirps with linear changing frequency, the following kernel seems to be suitable:

$$H_C(\nu;\tau) = \mathrm{e}^{-\frac{\tau^2}{4\pi^2\sigma}(\nu - 2\varepsilon\tau)^2}. \tag{3}$$

Figure 7 shows the numerically calculated TFD of the kernel (3) with $\varepsilon = \varepsilon_Z = 3983\,\mathrm{s}^{-2}$, $\sigma = 0.05$. The parameter ε controls the inclination of the frequency major axis of the kernel with the time axis [compare Figs. 7 and 1(b)!]. This inclination ψ was chosen for all components of the chirp according to the angular acceleration $\varepsilon = 0.5\tan(\psi)$.

Kernel (3) can be considered as a filter with time-dependent transmission frequency. It allows passing only those components of the ambiguity function, whose frequency changes with a steady speed ε. These components are the looked-for chirp components of the

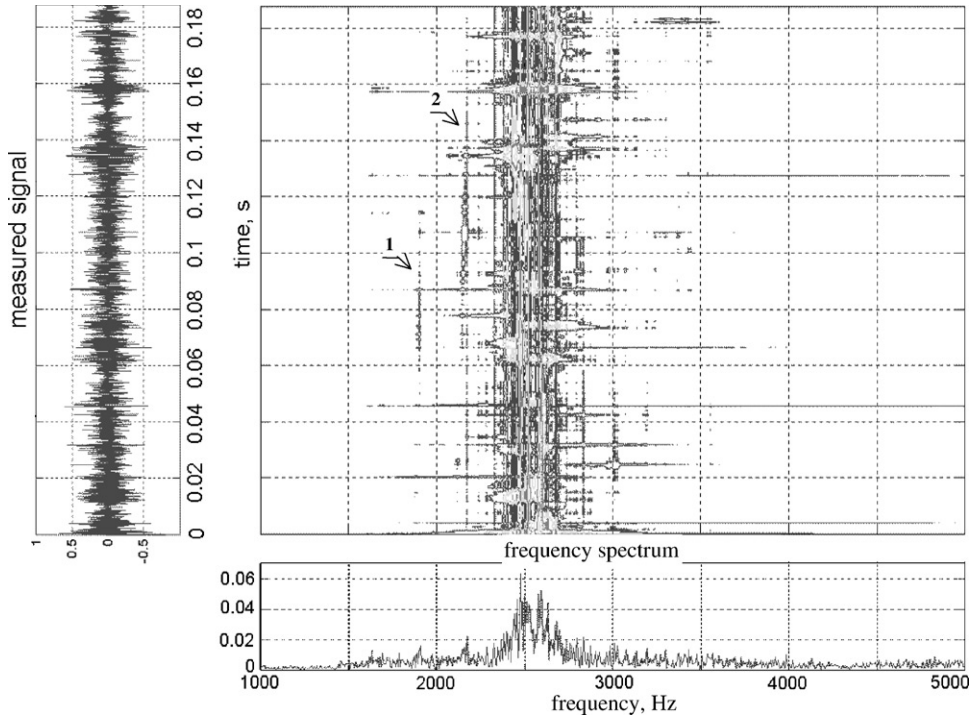

Figure 6. CWD with $\sigma = 0.05$ of the time-equidistant sampled measuring signal of gearbox acceleration during linear start up ('1' and '2' mark individual sidebands).

measured gearbox-structure-borne noise during a start-up with constant acceleration. After numerical weighting $A_x(\nu;\tau)H_C(\nu;\tau)$, these components will dominate the TFD. This can be seen in Fig. 8.

The lower part of Fig. 8 shows the ordinary frequency spectrum of the time function (left part in Fig. 8) of the weighted time series.

Now we see, as expected, the true time–frequency distribution, which was reached by combination of the advantages of the CWD (it means: the nearly total suppression of interference terms as well as a good resolution in time and frequency) and the respect to the non-stationarity of rotational speed of monitored gear.

The horizontal terms (transients) in the TFD (Fig. 8) have not changed in comparision with Figs. 4 and 6. This is why the kernel was not modified along the frequency axis.

The sideband structure, which is accepted as a robust symptom for the damage of teeth (and bearings also) can be better recognised, if the TFD is cleared of components, the significance of which for fault diagnostic until now is not investigated successfully. For suppression of the above-mentioned transient components (the horizontal lines in Figs. 4, 6 and 8) additional to the interference terms we created the following kernel:

$$H_{CM}(\nu;\tau) = \mathrm{e}^{-\frac{\alpha^2+\tau^2}{4\pi^2\sigma}(\nu-2\varepsilon\tau)^2}. \tag{4}$$

This kernel contains an additional parameter α besides ε [compare equations (4) and (3)!].The parameter α is responsible for the suppression of transient terms. As already stated in Section 2, these terms are spread out along the ν-axis in the ambiguity plane (see also references [12, 16]. Because of it, the new kernel is more narrow along this axis. This kernel, $H_{CM}(\nu;\tau)$, is shown in Fig. 9 for $\sigma = 0.05$, $\varepsilon = \varepsilon_Z = 3983\,\mathrm{s}^{-2}$ and $\alpha = 4.0$ [compare with the kernel $H_C(\nu;\tau)$ in Fig. 7!].

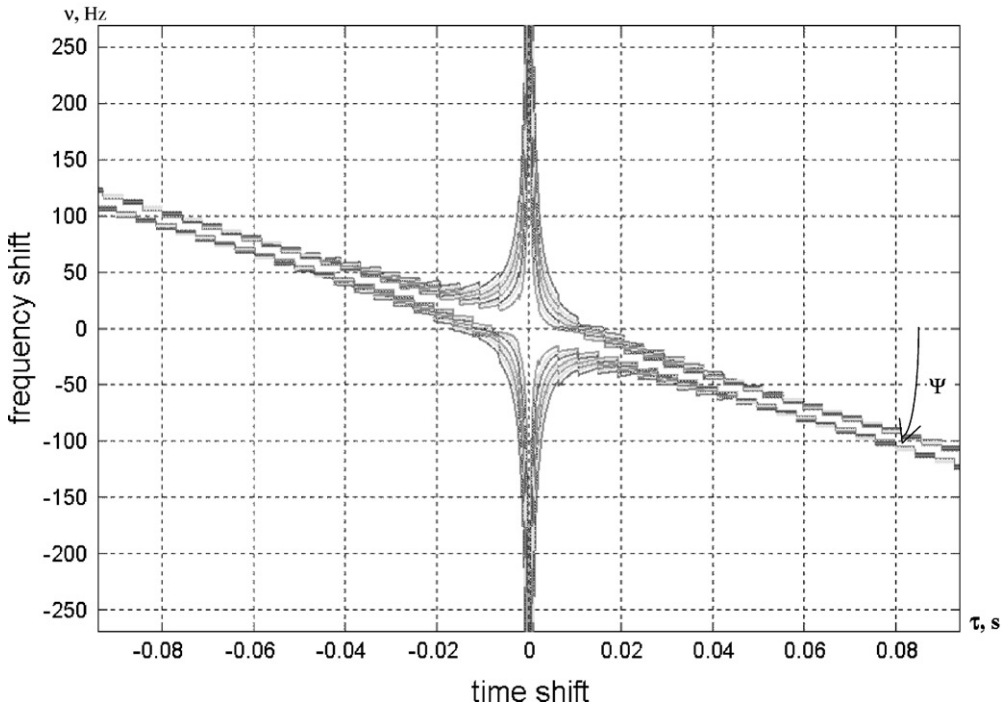

Figure 7. Kernel $H_C(v;\tau)$ at $\sigma = 0.05$, $\varepsilon = \varepsilon_Z = 3983\,s^{-2}$ for the time–frequency analysis of the time-equidistant sampled signal at linear start up of gear drive [$\varepsilon = 0.5 \cdot tan(\psi)$].

The CWD, which we executed by means of this kernel, shows an effective suppression of the impact-generated horizontal lines and were therefore more clear.

5.3. APPLICATION OF CONE-SHAPED AND ADAPTIVE SMOOTHING KERNELS

The application of the smoothing kernels according to equations (3) or (4), resp. implies the requirement of a constant and known-in-advance angular acceleration ε. Mostly, this parameter can be determined on the basis of the linear course of rotational speed laid down. If the angular acceleration is not known (but still constant), another construction of a signal-independent smoothing kernel is necessary. Two different approaches for this will be explained in the following section.

Cone-shaped kernels have a shape like a cone in the ambiguity plane [17, 18]. They are suitable for unsteady rotational speed with constant angular accelerations within a given limitation ε_K:

$$H_K(v;\tau) = \begin{cases} 1, & -2\varepsilon_k|\tau| \leqslant \leqslant v \leqslant 2\varepsilon_k|\tau|, \quad \varepsilon_K > 0 \\ 0 & \text{other} \end{cases} \tag{5}$$

Let us analyse the weighting performance of this kernel $H_K(v;\tau)$. From all terms of AF $A_x(v;\tau)$ of the measured signal $x(t)$ with angular accelerations $-\infty < \varepsilon < +\infty$ only those, for which $|\varepsilon| \leqslant \varepsilon_K$ will be kept. This property demands that the maximal angular acceleration during the course of rotational speed must be declared as limitation ε_K. In our case, we have to choose $\varepsilon_K = \varepsilon_Z$. The kernel (5) now allows passing of all vibrational signals which are generated by meshing of all damaged and undamaged teeth in the planetary set 2 of our gear drive. But all interference terms, which are situated inside the

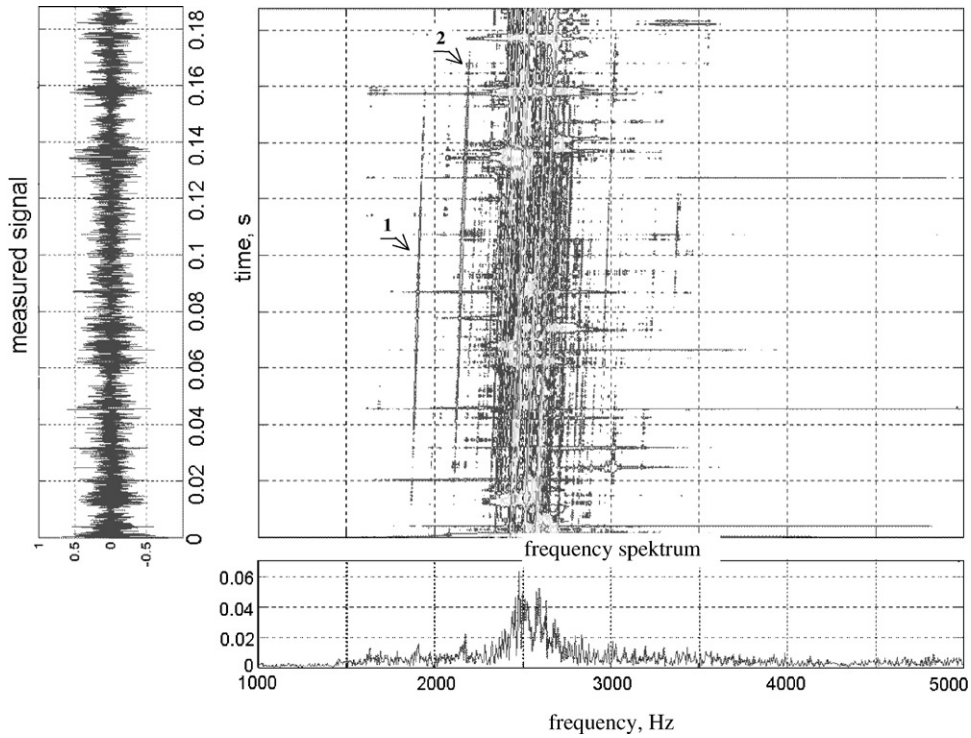

Figure 8. The time–frequency distribution $TFD_x(t;\omega)$ of the time-equidistant sampled measuring signal of gearbox during linear start up [weighted with the acceleration-respecting kernel $H_C(\nu;\tau)$; '1' and '2' mark individual sidebands].

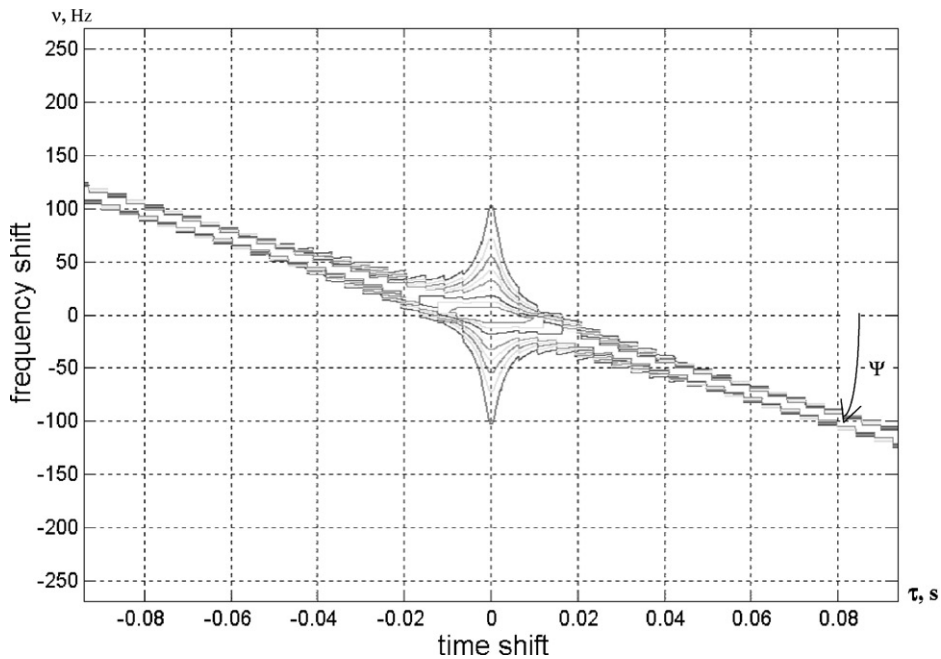

Figure 9. The modified kernel $H_C M(\nu;\tau)$ at $\sigma = 0.05$, $\varepsilon = \varepsilon_Z = 3983s^{-2}$ and $\alpha = 4.0$ for the time–frequency analysis of the time-equidistant sampled signal at linear start up of gear drive [$\varepsilon = 0.5\tan(\psi)$].

kernel cone $-2\varepsilon_K|\tau| \leqslant \nu \leqslant 2\varepsilon_K|\tau|$ in the ambiguity plane, can also pass this filter unfortunately. This is the main disadvantage of cone kernels.

More effective is the use of signal-dependent smoothing kernels [3, 19, 20]. Here, the parameter ε of the kernel function [see equation (3)] is adapted at the measured signal. By this, only the real vibration signal (meshing vibrations and sidebands) pass the 'filter', the interference terms are suppressed. There are known different approaches to design such kernels [19, 20]. Park and Kim [20] recommend the use of 'rotating windows'. It means that the symmetrical kernel according to Fig. 7 will be subjected to a change of angle $0^\circ \leqslant \psi < 180^\circ$ in the ambiguity plane. This position of ψ for which the smoothed integral (1) becomes maximal is looked for.

The algorithm of kernel adaption is the following [20]:

$$P_m \stackrel{!}{=} \max P(\psi), \quad -\pi/2 < \psi < \pi/2 \tag{6}$$

with

$$P(\psi) = \int_{-\infty}^{+\infty} \int_{-\infty}^{+\infty} |A_x(\nu;\tau) H(\nu;\tau;\psi)|^2 \, \mathrm{d}\tau \, \mathrm{d}\nu. \tag{7}$$

This algorithm was tested. There were used in equation (7) the AF $A_x(\nu;\tau)$ of the time-equidistant sampled signal and the kernel $H_C(\nu;\tau)$ (3). The relation between ε in equation (3) and ψ in equation (7) is $\boldsymbol{\varepsilon} = 0.5\tan(\psi)$. A variation of ε or ψ causes a rotation of one of the branches of the smoothing kernel in the ambiguity plane (see Fig. 7) around the crossing point of both branches.

Figure 10 shows the signal energy $P(\psi)$ *vs* ψ. A clear maximum of signal energy exists at the angular acceleration $\varepsilon = 4140\ \mathrm{s}^{-2}$. This quantity is in a very good correspondence with

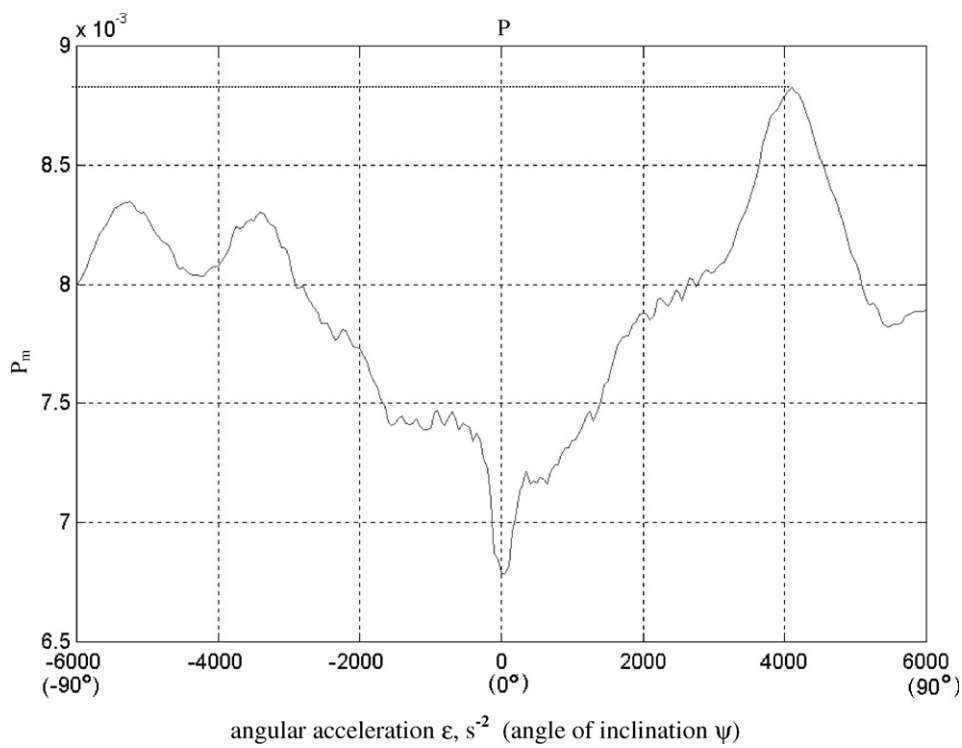

Figure 10. Signal energy P at different angular accelerations ε or angles of inclination ψ ($-90^\circ - +90^\circ$) of the smoothing kernel $H_C(\nu;\tau)$.

the exact angular acceleration of planet set 2 of our case-study gear, which amounts to $3983\,s^{-2}$ (see Section 5.2). The so-found quantity ε has to be used as parameter of the kernel (3) for the processing of the measured signal furthermore.

The combination of Choi–Williams distribution with the kernel adaption yields an efficient tool for side band analysis of unsteady operating gear drives also in the case of not-in-advance-known course of rotational speed. The only restriction is the linearity of increasing or decreasing of speed.

For consideration of non-linear changing rotational speed, there must be created another kind of smoothing kernels with adaptable structure and parameters [19, 21].

6. SUMMARY

This part of our paper is dedicated to the fault diagnosis of gear drives by means of the time–frequency analysis (TFA).

As a case study, we investigated a planetary gearing of a passenger car. The structure-borne noise was measured during the start-up, was followed by digitalisation and then numerically processed. The sampling was tuned by means of an incremental sender ('angle-equidistant') or by means of an ordinary impulse generator ('time-equidistant') alternatively.

For these time series which was sampled in equal intervals of rotational angles, the conventional methods of frequency analysis (Fourier-spectrum, Fourier-cepstrum) were just as well applicable as the time–frequency analysis of Cohen-class. This is why the angle-equidistant sampled signals are steady along the rotational angle axis. The result of processing is the ordering spectrum or the time-ordering distribution.

In the other approach—it means the time-equidistant sampling of measured signals—these methods of data processing were not appropriate. Therefore, we created and applied successfully new smoothing kernels for the Choi–Williams distribution according to the linear and known-in-advance course of rotational speed. By this, we get a new access to the fault diagnosis of machines with unsteady rotational speed.

With both approaches we detected and identified the faults at different tooth flanks. For the case of linear changing rotational speed, but without a priori knowledge of angular acceleration, we used a new procedure for optimisation of kernel parameters.

ACKNOWLEDGEMENTS

This research was supported by the Deutscher Akademischer Austauschdienst DAAD by awarding the postdoc-scholarship No. A/971/13553. An additional subvention was given by the State Ministry for Sciences and Art of Saxony. We thank Mr. D. Lieske for making the measurements.

REFERENCES

1. L. Cohen 1989 *Proceedings of the IEEE* **77**, 941–981. Time–frequency distributions—a review.
2. A. Mertins 1996 *Signaltheorie*. Stuttgart: Teubner.
3. F. Hlawatsch and G. F. Bourdeaux-Bartels 1992 *IEEE Signal Processing Magazine* **9**, 21–67. Linear und quadratic time–frequency signal representations.
4. H. Oehlmann, D. Brie, M. Tomczak and A. Richard 1997 *Mechanical System and Signal Processing* **11**, 529–545. A method for analysing gearbox faults using time-frequency representations.
5. W. J. Staszewski, K. Worden and G. R. Tomlinson 1997 *Mechanical System and Signal Processing* **11**, 673–692. Time–frequency analysis in gearbox fault detections using the Wigner-Ville distribution and pattern recognition.

6. F. K. Choy, V. Polyshchuk, R. J. Veillette and M. J. Braun 1997 *International Journal of Turbo and Jet Engines* **14**, 89–97. Health monitoring of a gear transmission using acoustic signatures.
7. W. J. Wang and P. D. McFadden 1995 *Mechanical System and Signal Processing* **9**, 497–507. Application of ortogonal wavelets to early gear damage detection.
8. S. T. Lin and P. D. McFadden 1997 *Mechanical System and Signal Processing* **11**, 603–609. Gear vibration analysis by b-spline wavelet-based linear wavelet transform.
9. M. Hildebrandt and G. Lechner 1992 *Maschinenmarkt, Würzburg* **98**, 42–46. Körperschall-Referenzsignale an Zahnradgetrieben analysieren.
10. Yu Ye Ivanov and G. Meltzer 1998 *Proceedings of the 3rd International Conference on Acoustical and Vibratory Surveillance Methods and Diagnostic Techniques* **1**, 333–343. Time-dependent cepstral analysis—its significance and application in technical diagnostics.
11. H.-I. Choi and W. Williams 1989 *IEEE Transactions on Acoustic, Speech and Signal Processing* **37**, 862-871. Improved time–frequency representation of multicomponent signals using exponential kernels.
12. S. Qian and D. Chen 1996 *Joint Time–Frequency Analysis: Methods and Applications*. Englewood Cliff, NJ: Prentice-Hall.
13. J. Jeong and W. J. Williams 1992 *IEEE Transactions on Signal Processing* **40**, 2608–2613. Mechanism of the cross-terms in spectrograms.
14. J. Kolerus 1995 *Zustandsüberwachung von Maschinen*. Sindelfingen: Expert-Verlag.
15. S. Braun 1986 *Mechanical Signature Analysis: Theory and Applications*. New York: Academic Press.
16. J. Jeong and W. J. Williams 1992 *IEEE Transactions on Signal Processing* **40**, 402–412. Kernel design for reduced interference distributions.
17. Y. Zhao, L. E. Atlas and R. J. Marks 1990 *IEEE Transactions on Acoustic, Speech and Signal Processing* **38**, 1084–1091. The use of cone-shaped-kernels for generalized time-frequency representations of nonstationary signals.
18. S. Oh and R. J. Marks 1992 *IEEE Transactions on Signal Processing* **40**, 1735–1744. Some properties of the generalized time–frequency representation with cone-shaped kernel.
19. R. G. Braniuk and D. L. Jones 1993 *IEEE Transactions on Signal Processing* **41**, 1589–1601. A signal-dependent time–frequency representation: optimal kernel design.
20. Y.-K. Park and Y.-H. Kim 1997 *Mechanical System and Signal Processing* **11**, 547–559. A method to minimise the cross-talk of the Wigner–Ville distribution.
21. D. L. Jones and T. W. Parks 1990 *IEEE Transactions on Acoustic, Speech and Signal Processing* **38**, 2127–2134. A high resolution data-adaptive time–frequency representation.